Interfacial instabilities in periodically driven Hele-Shaw flows

Eduardo O. Dias and José A. Miranda*
Departamento de Física, LFTC, Universidade Federal de Pernambuco, Recife, Pernambuco 50670-901, PE, Brazil
(Received 14 April 2009; revised manuscript received 15 June 2009; published 14 August 2009)

We consider flow in a Hele-Shaw cell for which the upper plate moves up and down, making the fluid-fluid interface be driven periodically. To study such a flow we employ a mode-coupling approach, which allows the analytical assessment of important aspects about the stability and morphology of the evolving interface. At the linear level, it is shown that both the amplitude and the frequency of the drive have a significant role in determining the ultimate number of fingers formed. The influence of these factors on the mechanisms of finger competition and finger tip behavior at the onset of nonlinear effects is also studied.

DOI: 10.1103/PhysRevE.80.026303 PACS number(s): 47.15.gp, 47.15.km, 47.20.Ma, 47.54.−r

I. INTRODUCTION

The Saffman-Taylor problem [1] considers the confined viscous flow between narrowly spaced parallel plates in Hele-Shaw cell geometry [2]. This famous pattern-forming problem involves the development of stable smooth fingers in long rectangular channels, or branched fronts if the flow takes place in open radial geometry [3]. Under such circumstances, the fluid motion is perfectly described by the well-known Darcy's law, which connects the fluid velocity to the pressure gradient.

Much of the research in this area has examined the flow in constant-gap spacing Hele-Shaw cells. However, a particularly interesting variation in the traditional Saffman-Taylor problem is the investigation of fingering instabilities in Hele-Shaw cells presenting variable-gap width. This can be accomplished by lifting (or compressing) the upper plate while the lower one remains at rest. To account for the variable-gap motion of the upper plate, the usual divergence-free condition for the flow velocity is modified so that the pressure field is no longer harmonic, and it satisfies a Poisson equation. These features differ significantly from the conventional constant-gap Hele-Shaw situation, in which the pressure is Laplacian and where a divergence-free condition holds. The study of fingering pattern formation under time-dependent gap conditions is very diverse, involving the lifting of Newtonian [4], non-Newtonian [5], miscible [6], and magnetic fluids [7]. In addition to being an intrinsically important academic problem, the lifting Hele-Shaw cell system is also intimately related with the practical problem of adhesion [8–10].

A curious but still largely unexplored gap-variable Hele-Shaw situation has been examined in Ref. [11] that considered the case in which the upper cell plate oscillates sinusoidally. A generalized effectively two-dimensional (2D) Darcy's law has been derived, taking into account part of the inertial terms in the three-dimensional (3D) Navier-Stokes equation, and a linear stability calculation was presented. Experiments considering compressible flow situations have also been performed, mostly by taking the inner (outer) fluid as air (water), revealing the formation irregular fingering structures. The case in which both fluids are incompressible has only been addressed by numerical solutions of the governing equations. Unfortunately, the inclusion of inertia resulted in complicated linear stability expressions, which cannot be solved in closed form. In fact, not even an explicit expression for the linear dispersion relation of the system has been found in Ref. [11]. This has obscured the possibility of extracting more relevant information at linear and nonlinear stages of the dynamics.

It turns out that the periodically driven Hele-Shaw problem originally proposed in Ref. [11] can be significantly simplified if a related but still interesting case is considered in which inertial effects are neglected. In the context of Hele-Shaw flow problems, the role of inertia is quantified by a Reynolds number (relative measure of inertial and viscous forces), which is directly proportional to the cell gap thickness, and inversely proportional to the viscosity of the displaced fluid. Since most experimental and theoretical studies of the Saffman-Taylor instability deal with very thin cell gaps and highly viscous oils, the vanishing Reynolds number limit is readily validated [1–10]. By considering such a limit, we show that both the linear stability analysis and the weakly nonlinear dynamics of the system can be accessed so that a number of useful results can be deduced analytically and in closed form. In this work, we perform a systematic study of the linear and early nonlinear behavior of the viscous fingering patterns under a periodically driven excitation. Our analytical findings are rationalized by focusing on a mode-coupling description of the Saffman-Taylor problem [12] adapted to the variable-gap Hele-Shaw situation.

II. PHYSICAL PROBLEM AND GOVERNING EQUATIONS

The geometry of the periodically driven Hele-Shaw cell problem is sketched in Fig. 1. Consider a vibrating Hele-Shaw cell of gap width b containing two immiscible incompressible viscous fluids. The upper plate of the cell is allowed to move up and down along the z axis, which is perpendicular to the cell plates. The coordinate system is defined in such a way that its origin is located at the center of the cell. On the other hand, the lower plate is hold fixed at $z=0$. The initial plate-plate distance is represented by b_0 and the initial fluid-fluid interface is circular, having radius R_0. The upper plate is sinusoidally driven as $b(t)=b_0$

*jme@df.ufpe.br

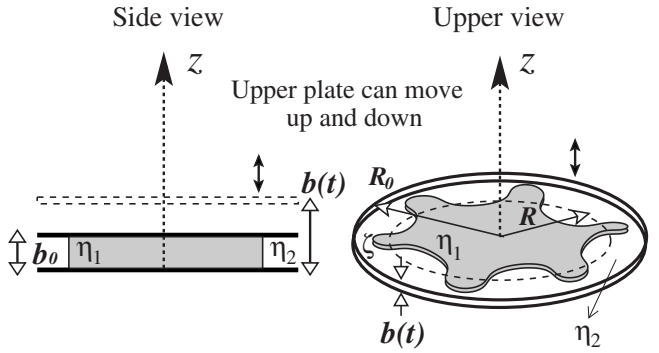

FIG. 1. Diagrammatic representation of the periodically driven flow in a variable-gap width Hele-Shaw cell.

$+b_1 \sin(\omega t)$, where b_1 denotes the oscillation amplitude, and ω is the angular frequency. The viscosities of the inner and outer fluids are, respectively, denoted as η_1 and η_2, and the surface tension between them is σ. The perturbed interface is described as $\mathcal{R}(\theta,t)=R(t)+\zeta(\theta,t)$, where $\zeta(\theta,t)=\Sigma_{n=-\infty}^{+\infty}\zeta_n(t)\exp(in\theta)$ represents the net interfacial perturbation in polar coordinates (r,θ) with Fourier amplitudes $\zeta_n(t)$, and discrete azimuthal wave numbers n. $R=R(t)$ is the time-dependent unperturbed radius of the fluid-fluid interface. Note that conservation volume leads to the useful relation $R^2b=R_0^2b_0$.

Our analytical approach follows a theoretical model proposed in Refs. [4,11,12], and considers that the fluid flow is governed by the continuity equation for incompressible fluids

$$\nabla \cdot \mathbf{u}_j = 0, \tag{1}$$

and by the Navier-Stokes equation

$$\rho_j\left[\frac{\partial \mathbf{u}_j}{\partial t} + (\mathbf{u}_j \cdot \nabla)\mathbf{u}_j\right] = -\nabla p_j + \eta_j \nabla^2 \mathbf{u}_j, \tag{2}$$

where $\mathbf{u}_j$ denotes the three-dimensional fluid velocity for fluid j (where $j=1,2$), ρ_j represent the densities of the fluids, and p_j is the hydrodynamic pressure.

For the quasi-two-dimensional geometry of the Hele-Shaw cell, one reduces the three-dimensional flow to an equivalent two-dimensional one by averaging Eqs. (1) and (2) over the direction perpendicular to the plates. By performing the gap averaging of Eq. (1) one obtains a modified incompressibility condition

$$\nabla \cdot \mathbf{v} = -\frac{\dot{b}(t)}{b(t)}, \tag{3}$$

where the overdot denotes total time derivative, ∇ represents the two-dimensional gradient operator in polar coordinates, and $\mathbf{v}(r,\theta)=\int_0^b \mathbf{u}(r,\theta,z)dz/b$. By applying the same procedure to Eq. (2), and by neglecting the inertial terms as in Refs. [1–10], one obtains Darcy's law

$$\mathbf{v}_j = -\frac{b(t)^2}{12\eta_j}\nabla p_j. \tag{4}$$

We point out that the use of Eq. (4) implies that we assume that the upper plate is not being lifted high enough to alter the system being of large aspect ratio $[R(t) \gg b(t)]$. A discussion about the range of applicability of Darcy's law approach to our system is presented in the Appendix.

From Eq. (3) it can be verified that the equation satisfied by the velocity potential ϕ $(\mathbf{v}=-\nabla\phi)$ differs from Laplace equation valid in the usual constant-gap Hele-Shaw flow so that here the velocity potential is not a harmonic function

$$\nabla^2 \phi_j = \frac{\dot{b}(t)}{b(t)}. \tag{5}$$

However, since the gap is only time dependent, the solution of Poisson equation (5) can be conveniently expressed as

$$\phi_j = \phi_j^0 + \sum_{n\neq 0} \phi_{jn}\left(\frac{R^{|n|}}{r^{|n|}}\right)^{(-1)^j} \exp(in\theta) + \frac{\dot{b}r^2}{4b}, \tag{6}$$

where the first two terms at the right-hand side represent the solution of the Laplace equation for ϕ (with ϕ_j^0 being independent of r and θ), while the last term is the radial particular solution of Eq. (5).

By rewriting Darcy's law (4) in terms of the velocity potential for each fluid, and then by subtracting the resulting expressions, we obtain the equation of motion for the system evaluated at the fluid-fluid interface

$$\left[A\frac{(\phi_1+\phi_2)}{2} + \frac{(\phi_1-\phi_2)}{2}\right] = \frac{b^2(p_1-p_2)}{12(\eta_1+\eta_2)}, \tag{7}$$

where $A=(\eta_1-\eta_2)/(\eta_1+\eta_2)$ is the viscosity contrast.

The problem is then specified by the usual pressure jump boundary condition

$$p_1 - p_2 = \sigma\kappa, \tag{8}$$

where κ represents the interfacial curvature, plus the kinematic boundary condition, which states that the normal components of each fluid's velocity are continuous at the interface

$$\mathbf{n}\cdot\nabla\phi_1 = \mathbf{n}\cdot\nabla\phi_2, \tag{9}$$

where $\mathbf{n}=\nabla[r-\mathcal{R}(\theta,t)]/|\nabla[r-\mathcal{R}(\theta,t)]|$ denotes the unit normal vector at the interface. Note that this last equation is useful in expressing ϕ_j in terms of ζ_n and $\dot{\zeta}_n$.

To obtain an equation of motion for the perturbation amplitudes valid at linear and early nonlinear stages, first we Fourier expand the velocity potentials in Eq. (6) and the interfacial curvature κ in Eq. (8) to second order in ζ. Then we substitute all these expanded second-order expressions back into Eq. (7), and Fourier transform it to obtain a dimensionless differential equation for the evolution of the system (for $n\neq 0$)

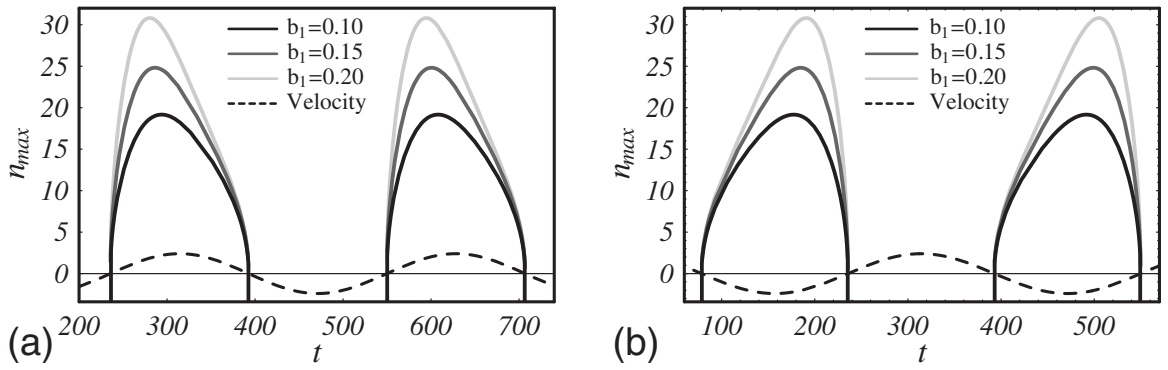

FIG. 2. $n_{\max}$ as a function of the dimensionless time t, for (a) $A=+1$, (b) $A=-1$, and different values of the dimensionless amplitude b_1 (solid curves). The black dashed curve illustrates as the velocity of the upper plate $\dot{b}$ (not in scale) varies with t. Here $q=200$ and $\Omega=0.02$.

$$\dot{\zeta}_n = \lambda(n)\zeta_n + \sum_{n' \neq 0} [F(n,n')\zeta_{n'}\zeta_{n-n'} + G(n,n')\dot{\zeta}_{n'}\zeta_{n-n'}], \tag{10}$$

where

$$\lambda(n) = \frac{\dot{b}}{2b}(A|n| - 1) - \frac{8b^{7/2}}{q^3}|n|(n^2 - 1) \tag{11}$$

is the linear growth rate, and $q=2R_0/b_0$ denotes the initial aspect ratio.

The second-order mode-coupling terms are given by

$$F(n,n') = \frac{\dot{b}}{b^{1/2}}\left[A|n|\left(\mathrm{sgn}(nn') - \frac{1}{2}\right) - 1\right] - \frac{16b^4}{q^3}|n|\left[1 - \frac{n'}{2}(3n' + n)\right], \tag{12}$$

and

$$G(n,n') = 2b^{1/2}\{A|n|[\mathrm{sgn}(nn') - 1] - 1\}. \tag{13}$$

In Eq. (10) in-plane lengths, $b(t)$, and time are rescaled by $2R_0$, b_0, and the characteristic time $T=[12b_0(\eta_1+\eta_2)]/\sigma$, respectively. The dimensionless gap thickness is written as $b(t)=1+b_1 \sin \Omega t$, where the dimensionless angular frequency parameter is represented as $\Omega=[12\omega b_0(\eta_1+\eta_2)]/\sigma$. Without loss of generality we focus on the high viscosity contrast cases $A=+1$ and $A=-1$. We stress that from now on we work with the dimensionless version of the equations.

It is worth pointing out that all dimensionless parameters we use throughout this work are as close as possible to the typical experimental quantities utilized in Ref. [11]. Although the experimental value of the surface tension σ is not given in Ref. [11], in evaluating the dimensionless parameter Ω, we assumed that $\sigma=O(10^{-3})-O(10^{-2})$ N/m. The frequencies of the drive we utilized are $0<f\leq 60$ Hz, where $f=\omega/2\pi$.

III. LINEAR REGIME: STABILITY ANALYSIS

We begin our study by using Eq. (11) to examine how the development of interfacial instabilities at linear stages of the pattern evolution could be modified by the influence of b_1 and Ω. At the linear level important information can be extracted from a quantity obtained by setting $d\lambda(n)/dn=0$, yielding

$$n_{\max} = \sqrt{\frac{1}{3}\left(1 + \frac{\dot{b}Aq^3}{16b^{9/2}}\right)}. \tag{14}$$

A quantity closely related to $n_{\max}$ is the so-called fastest growing mode n^*, defined as the *integer* mode that produces the largest growth rate. A given mode n is only the fastest growing when $\lambda(n)>\lambda(n-1)$ and $\lambda(n)>\lambda(n+1)$. This is the mode that will tend to dominate during the early stages of the pattern formation process and will perhaps determine the typical number of fingers at later stages. So, by examining the time evolution of $n_{\max}$ we can access how the typical number of interfacial fingering structures vary as the upper plate of the Hele-Shaw cell oscillates.

Figure 2 plots $n_{\max}$ as a function of time t for different values of the oscillation amplitude b_1: 0.10, 0.15, and 0.20. In Fig. 2(a) the more viscous fluid is the inner one ($A=+1$), while in Fig. 2(b) the more viscous fluid is the outer fluid ($A=-1$). To better guide the eye regarding the stability of the interface, the velocity of the upper plate $\dot{b}=b_1\Omega \cos \Omega t$ is also shown, represented by a black dashed curve (not in scale). Characteristic values $q=200$ and $\Omega=0.02$ have been used in Fig. 2. Notice that there is nothing special about the dimensionless time interval we used to plot Fig. 2 and other figures in this work. After all, the functions involved in these graphs are periodic so that the choice of the time interval is quite arbitrary.

First, we examine the situation in which the more viscous fluid is the inner one [Fig. 2(a)]. The interfacial instability is driven by the viscosity difference between the fluids, similarly to the usual Saffman-Taylor problem. If the upper plate is lifted ($\dot{b}>0$) the outer less viscous fluid penetrates the inner more viscous one, resulting in an unstable interface with a certain number of fingers. Conversely, if the upper plate moves downward ($\dot{b}<0$) the interface is linearly stable and no fingers are formed. This behavior can be easily verified by observing the black dashed curve representing $\dot{b}$: in-

creasingly larger (positive) velocities lead to a larger number of fingers. Moreover, notice that the time variation in the number of fingers is directly related to the acceleration $\ddot{b}$ of the oscillatory plate. If the plate accelerates ($\dot{b}$ and $\ddot{b}$ have the same sign) the number of fingers tends to increase with time. Nevertheless, if the plate decelerates $n_{\max}$ decreases with time. The role of oscillation amplitude b_1 is also evident: as b_1 is increased we observe that more and more fingers result within the region in which $\dot{b}>0$. On the other hand, despite the destabilizing action of b_1, no fingers arise if $\dot{b}<0$.

Now we turn to the case in which the more viscous fluid is the outer one [Fig. 2(b)]. In contrast to what we have seen in Fig. 2(a), notice that now the fingers arise when $\dot{b}<0$. Despite this fact, similarly to what occurred in Fig. 2(a) we can see that larger b_1 imply an increase in the number of fingers.

A curious feature of Fig. 2(b) is the fact that the curves describing $n_{\max}$ tend to deviate to the right as b_1 is increased. This is in contrast to the behavior depicted in Fig. 2(a) where the curves move to the left. This asymmetry indicates that in general $n_{\max}$ is not maximized at the point of maximum velocity. But why do the $n_{\max}$ curves deviate toward shorter (longer) times for $A=+1$ ($A=-1$) as b_1 is increased? The answer to this question can be obtained if we use Eq. (14) to evaluate the time $t=\tau$ at which $n_{\max}$ reaches its highest magnitude

$$\sin \Omega\tau = \frac{1-\sqrt{1+63b_1^2}}{7b_1}. \tag{15}$$

Note that for a given Ω the time τ only depends on b_1, showing no dependence on A. This might sound as an apparent contradiction since we know from Figs. 2(a) and 2(b) that we have distinct behaviors for the deviation in $n_{\max}$ for $A=+1$ and $A=-1$. In fact, there is no contradiction here. First, notice from Eq. (15) that as $b_1\to 0$, $\sin \Omega\tau\to 0$, implying that the highest magnitude of $n_{\max}$ occurs exactly at the time in which the velocity of the plate $\dot{b}$ is maximized. Note that in this particular situation there is no asymmetry.

The asymmetry will arise for the cases involving larger values of b_1. Again from Eq. (15) we observe that for such values of the oscillation amplitude $\sin \Omega\tau<0$. For $A=+1$ we know that the fingers become unstable when $\sin \Omega t$ varies from -1 to $+1$. So, as $n_{\max}$ is largest for negative values of $\sin \Omega\tau$, this situation would occur at shorter times, deviating the curves in Fig. 2(a) to the left. On the other hand, for $A=-1$, since Eq. (15) is independent of A we can say the value of $\sin \Omega\tau$ remains unaltered. However, for $A=-1$ the fingers become unstable when $\sin \Omega t$ varies from $+1$ to -1 so that $n_{\max}$ is maximized at longer times, deviating the curves shown in Fig. 2(b) to the right.

We also examined how $n_{\max}$ responds to changes in driving frequency Ω for a given value of amplitude b_1. This aspect is illustrated in Fig. 3, which plots $n_{\max}$ as a function of time t, for $A=-1$, $b_1=0.15$, and two different frequencies $\Omega=0.01$ (black solid curves) and $\Omega=0.02$ (gray solid curves). The velocity curves corresponding to these two frequencies present the same color labeling but are represented

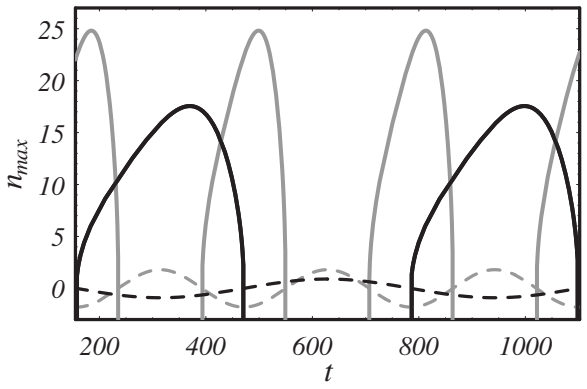

FIG. 3. $n_{\max}$ as a function of time t, for $A=-1$, $b_1=0.15$, $q=200$, and two values of the frequency: $\Omega=0.01$ (black solid curves) and $\Omega=0.02$ (gray solid curves). The dashed curves illustrate how the upper plate velocity $\dot{b}$ (not in scale) varies with time for each Ω taken.

by dashed curves. As expected, as $A=-1$ we only have fingers when $\dot{b}<0$. It is also evident that the periodicity of $n_{\max}$ is always the same as the periodicity of the plate oscillation. We observe that higher frequencies result in the production of a larger number of fingers. This can be readily justified by inspecting Eq. (14): larger Ω induces higher velocity $\dot{b}$, which leads to increased $n_{\max}$. Moreover, the time interval for which the fingers show up at the interface is decreased for larger values of the frequency Ω. This is connected to the increase in the plate's acceleration $\ddot{b}$ as Ω is increased. We note that similar conclusions would be reached if $A=+1$, the only difference being that in this case the fingers would appear as deviated to the left.

Another important quantity can be extracted from the linear growth rate given by Eq. (11). It refers to the critical driving amplitude b_1^{crit}, which is required to excite a given mode n. This quantity is obtained by setting $\lambda(n)=0$. The response of b_1^{crit} to frequency Ω is illustrated in Fig. 4 for $A=-1$, three values of $n=10,20,30$, and two different initial aspect ratios $q=180,200$. The time considered is $t=200$. This graph works like a linearized phase portrait for the system. For a given n, we clearly see that larger values of Ω lead to smaller b_1^{crit}. Therefore, we can say that higher Ω make it

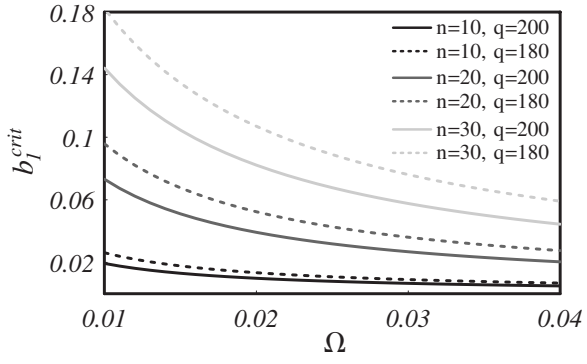

FIG. 4. Critical driving amplitude b_1^{crit} as a function of Ω, for $A=-1$, mode numbers $n=10,20,30$, and initial aspect ratio $q=180,200$. We set $t=200$.

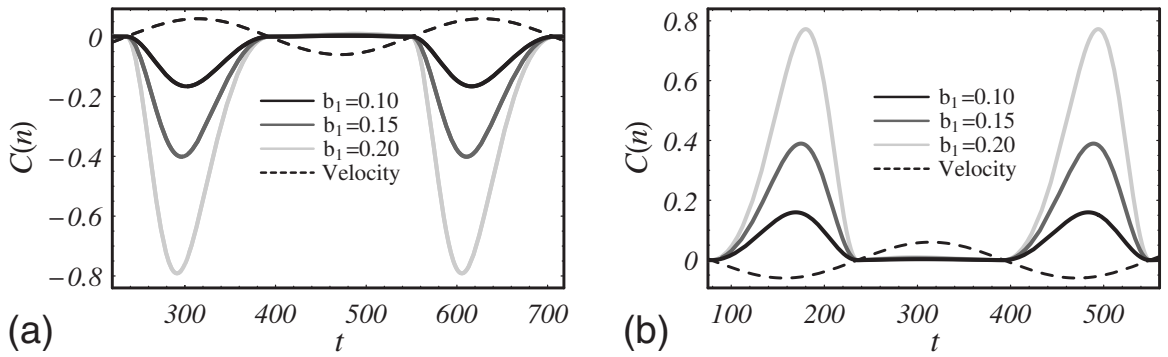

FIG. 5. Behavior of the finger competition function $C(n)$ as time is varied for the cases (a) $A=+1$ and (b) $A=-1$. Three different values of the oscillation amplitudes b_1 are considered (solid curves), $q=200$, and $\Omega=0.02$. The upper plate velocity $\dot{b}$ (not in scale) is illustrated by the dashed curve.

easier to excite a given interfacial mode. This reinforces the destabilizing character of the frequency, as we have discussed in Fig. 2. On the other hand, as the solid curves lie below the dashed ones, it is also evident that larger q (smaller initial gap spacing) leads to more unstable situations. Note that the influence of q in determining the stability of the interface is more significant for larger n. Once again, a qualitatively similar behavior is observed if $A=+1$.

IV. WEAKLY NONLINEAR REGIME: GROWTH MECHANISMS AND PATTERN MORPHOLOGY

It is well known that the basic growth mechanisms of the viscous fingering problem are finger competition and finger tip splitting or finger tip narrowing [2]. These mechanisms characterize the morphology of the patterns and are intrinsically nonlinear. So, in order to systematically investigate the main morphological features of the emerging fingering patterns in periodically driven Hele-Shaw flows, one must go beyond purely linear analysis. To do that we now turn our attention to the weakly nonlinear flow stage, and focus on the onset of nonlinear effects.

Despite the somewhat complicated nature of second-order mode-coupling equation (10), valuable information can be extracted from it by examining the coupling of a small number of Fourier modes. To simplify our discussion we rewrite Eq. (10) in terms of cosine and sine modes, where the cosine $a_n=\zeta_n+\zeta_{-n}$ and sine $b_n=i(\zeta_n-\zeta_{-n})$ amplitudes are real valued. For consistent second-order expressions, we replace the time derivative terms on the right-hand side of Eq. (10) as $\dot{a}_n$ and $\dot{b}_n$ by $\lambda(n)a_n$ and $\lambda(n)b_n$, respectively. Without loss of generality we choose the phase of the fundamental mode so that $a_n>0$ and $b_n=0$. Throughout our analysis we will assume that the fundamental mode n coincides with the fastest growing mode n^*.

We begin by discussing finger competition events. We follow Ref. [12] and consider finger length variability as a measure of the competition among fingers. Within our approach the finger competition mechanism can be described by the influence of a fundamental mode n, assuming n is even, on the growth of its subharmonic mode $n/2$. The correctness and accuracy of this simple finger competition mechanism has been extensively tested by sophisticated numerical simulations [13,14]. The equations of motion for the subharmonic mode can be written as

$$\dot{a}_{n/2}=\{\lambda(n/2)+C(n)a_n\}a_{n/2}, \tag{16}$$

$$\dot{b}_{n/2}=\{\lambda(n/2)-C(n)a_n\}b_{n/2}, \tag{17}$$

where the finger competition function is given by

$$C(n)=\frac{1}{2}\left[F\left(-\frac{n}{2},\frac{n}{2}\right)+\lambda(n/2)G\left(\frac{n}{2},-\frac{n}{2}\right)\right]. \tag{18}$$

Observing Eqs. (16) and (17) we verify that $C(n)>0$ increases the growth of the cosine subharmonic $a_{n/2}$ while inhibiting growth of its sine subharmonic $b_{n/2}$. The result is an increased variability among the lengths of fingers of fluid 1 penetrating into viscous fluid 2. This effect describes finger competition. Sine modes $b_{n/2}$ would vary the lengths of fingers of fluid 2 penetrating into fluid 1 but it is clear from Eq. (17) that their growth is suppressed. Reversing the sign of $C(n)$ would exactly reverse these conclusions, such that modes $b_{n/2}$ would be favored over modes $a_{n/2}$. Regardless of its sign, the magnitude of the function $C(n)$ measures the strength of the competition: increasingly larger values of $C(n)$ lead to enhanced finger competition.

By examining Fig. 5(a) we notice that $C(n)<0$ if $A=+1$. However, by inspecting Fig. 5(b) we observe that $C(n)>0$ if $A=-1$. This means that, regardless of the sign of the viscosity contrast, we have increased competition among the fingers of the less viscous fluid. At the same time, competition among the fingers of the more viscous is restrained. Of course, these results could not be guessed by purely linear analysis. Moreover, it is also clear that the strength of the competition is considerably sensitive to changes on the oscillation amplitude: larger values of b_1 lead to increasingly stronger finger competition. Finally, we can also verify both for $A=+1$ and $A=-1$ that there exists a trend to enhanced competition for larger values of the upper plate velocity. We have also analyzed the influence of the frequency Ω (for a fixed value of b_1) and found that finger competition increases significantly for larger values of Ω.

Similarly to what we have observed in Figs. 2 and 3, in Fig. 5 we see that the time for which $C(n)$ takes a minimum

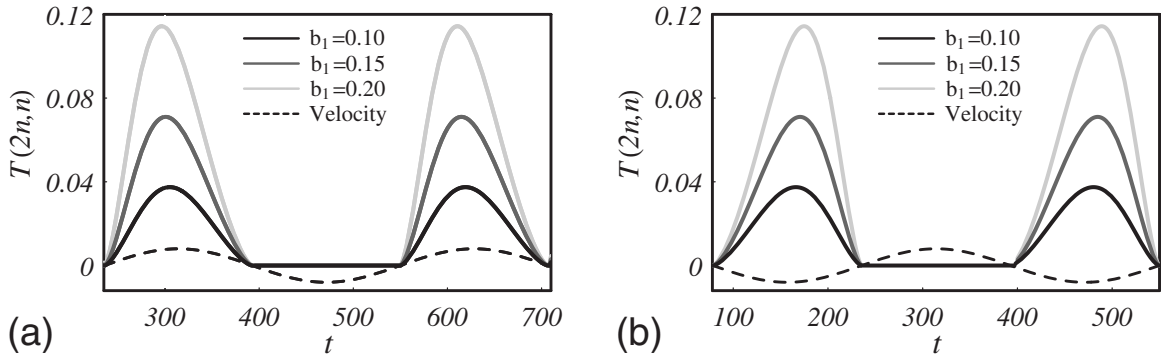

FIG. 6. Behavior of the finger tip function $T(2n,n)$ as time is varied for the cases (a) $A=+1$ and (b) $A=-1$. Three different values of the oscillation amplitudes b_1 are considered (solid curves), $q=200$, and $\Omega=0.02$. The upper plate velocity $\dot{b}$ (not in scale) is illustrated by the dashed curve.

or a maximum value is deviated from the time when the upper plate velocity takes maximum or minimum values. In order to calculate either the maximum or the minimum of the finger competition function (which is a function of $n=n_{\max}$ and t), we have that

$$\frac{dC(n_{\max},t)}{dt} = \frac{\partial C(n_{\max},t)}{\partial t} + \frac{\partial C}{\partial n_{\max}}\frac{dn_{\max}}{dt} = 0. \tag{19}$$

We have verified numerically that $\partial C/\partial n_{\max}$ is always nonzero as time processes, and its sign remains unchanged: $\partial C/\partial n_{\max}<0$ and $C(n)<0$ if $A=+1$, and $\partial C/\partial n_{\max}>0$ and $C(n)>0$ if $A=-1$. Therefore, an increase in the number of fingers ($dn_{\max}/dt>0$) produces an increase in the magnitude of the competition. Likewise, a decrease in $n_{\max}$ results in a diminished magnitude of $C(n)$. This leads to a similar deviation in $C(n)$ as the one that occurred in $n_{\max}$. The influence of the term $\partial C/\partial t$ is to inhibit this deviation. A similar behavior will also be observed in Fig. 6.

We close this section by investigating finger tip behavior. Finger tip-splitting and finger tip-narrowing phenomena are described by considering the influence of a fundamental mode n on the growth of its harmonic $2n$ [12]. The equations of motion for the harmonic mode are

$$\dot{a}_{2n} = \lambda(2n)a_{2n} + T(2n,n)a_n^2, \tag{20}$$

$$\dot{b}_{2n} = \lambda(2n)b_{2n}, \tag{21}$$

where the finger tip function is defined as

$$T(2n,n) = \frac{1}{2}[F(2n,n) + \lambda(n)G(2n,n)]. \tag{22}$$

Since the growth of the sine mode b_{2n} is uninfluenced by a_n and does not present second-order couplings, we focus on the growth of the cosine mode a_{2n} as given by Eq. (20). It shows that the presence of the fundamental mode n forces growth of the harmonic mode $2n$. The function $T(2n,n)$ acts like a driving force and its sign dictates finger tip behavior. If $T(2n,n)<0$, a_{2n} is driven negative, the sign that leads to finger tip broadening and finger tip splitting. Conversely, if $T(2n,n)>0$ growth of $a_{2n}>0$ would be favored, leading to outward-pointing finger tip narrowing.

Figure 6 depicts how the function $T(2n,n)$ varies with t, for (a) $A=+1$, and (b) $A=-1$. All the remaining physical parameters are exactly equal to the ones used in Fig. 5. It is evident that, independently of the value of A, $T(2n,n)\geq 0$. Therefore, one should not expect the existence of finger tip splitting in this periodically driven Hele-Shaw flow. Instead, we should observe fingers that should appear relatively narrow at their tips. Since this mechanism refers to the outward moving fingers of the inner fluid, in Fig. 6(a) the fingers affected are the ones of the more viscous fluid, whereas in Fig. 6(b) the fingers that become narrower are those of the less viscous fluid. Finally, note that this finger tip behavior is intensified for larger oscillation amplitudes.

V. CONCLUSION

We have studied the linear stability and the weakly nonlinear dynamics of a fluid-fluid interface, which is driven periodically through the vibration of a Hele-Shaw cell's upper plate. Our study was motivated by a previous investigation performed by Rauseo [11] who analyzed a general case in which inertial contributions have been taken into account. Regrettably, the inclusion of such inertial effects defies the analytical treatment of the problem, even at early linear stages of the interface evolution. By neglecting the troublesome inertial contributions we have shown that the problem could be approached analytically through a mode-coupling theory. In that way we were able to carry out a more detailed stability analysis than presented for the more general case studied in [11]. In addition, key morphological properties of the interface have also been probed at the onset of nonlinear effects.

At the linear level, we have verified that both the oscillation amplitude b_1 and the frequency of the drive Ω have important roles in determining the stability of the interface, particularly the number of emerging interfacial fingers. Intrinsically nonlinear growth mechanisms related to finger competition and finger tip behavior have also been examined. We have detected an increased competition among the fingers of the less viscous fluid, independently of the value of the viscosity contrast A. In addition, enhanced competition is favored for larger b_1 and Ω. Finally, our model predicts the

suppression of finger tip-splitting phenomena in such periodically driven flows.

Unfortunately, a quantitative comparison between our theoretical results and the compressible flow experiments performed in Ref. [11] was not possible, mostly due to the lack of detailed experimental data for the incompressible flow situation we have studied. However, we hope that experimentalists will feel motivated to perform a more systematic comparison in the future. In the laboratory the periodically driven system we examined here provides a convenient controllable manner of investigating pattern formation processes by varying, for instance, the frequency or amplitude of oscillation.

ACKNOWLEDGMENTS

J.A.M. thanks CNPq (Brazilian Research Council) for financial support of this research through the program "Instituto Nacional de Ciência e Tecnologia de Fluidos Complexos (INCT-FCx)," and also through the CNPq/FAPESQ Pronex program. E.O.D. wishes to thank CNPq for financial support.

APPENDIX: RANGE OF APPLICABILITY OF DARCY'S LAW APPROACH

This Appendix presents a discussion about the validity of our Darcy's law formulation for periodically driven Hele-Shaw flows. We begin by following Ref. [11], which presents a more general form for Darcy's law equation (4) {see Eq. (4) in Ref. [11]} written for a given fluid

$$\left[\rho\frac{\partial \mathbf{v}}{\partial t}+\rho\frac{\dot{b}(t)}{b(t)}\mathbf{v}+\frac{12\eta}{b(t)^2}\mathbf{v}\right]=-\boldsymbol{\nabla}p. \tag{A1}$$

In contrast to the majority of studies in Hele-Shaw flows [1–10] the gap-averaged equation (A1) includes part of the inertial terms originally present in Navier-Stokes equation (2). In deriving Eq. (A1) Rauseo neglected the advective inertial term $(\mathbf{u}\cdot\boldsymbol{\nabla})\mathbf{u}$, but kept the unsteady inertial term $\partial\mathbf{u}/\partial t$ during the gap-averaging process. The two initial terms on the left-hand side of Eq. (A1) are originated from the unsteady inertial contribution. For a full derivation and discussion of Eq. (A1) we refer the reader to Rauseo's work [11].

By using the same rescaling we have utilized in our work, Eq. (A1) can be rewritten in a dimensionless form as

$$\frac{\mathrm{Re}}{\Omega}\left[\frac{\partial \mathbf{v}}{\partial t}+\frac{\dot{b}(t)}{b(t)}\mathbf{v}\right]+\frac{12}{b(t)^2}\mathbf{v}=-\boldsymbol{\nabla}p, \tag{A2}$$

where the important dimensionless parameter

$$\mathrm{Re}=\frac{\rho b_0^2\omega}{\eta} \tag{A3}$$

represents a Reynolds number, and $\Omega=[12\omega b_0\eta]/\sigma$. The Reynolds number conveniently works as a controlling parameter that regulates the strength of the inertial effects.

By using Eq. (A2) we obtain the following condition for the neglect of the inertial effects

$$\left|\frac{\mathrm{Re}}{\Omega}\left[\frac{\partial \mathbf{v}}{\partial t}+\frac{\dot{b}(t)}{b(t)}\mathbf{v}\right]\right|\ll\left|\frac{12}{b(t)^2}\mathbf{v}\right|. \tag{A4}$$

An estimate for the condition of validity [Eq. (A4)] can be obtained by considering the evolution of a purely circular domain and the incompressible nature of the flow as given by Eq. (3), yielding a relation between the upper plate and the interface velocities

$$\mathbf{v}=\dot{R}\hat{\mathbf{r}}=-\frac{\dot{b}(t)R(t)}{2b(t)}\hat{\mathbf{r}}, \tag{A5}$$

where $\hat{\mathbf{r}}$ denotes the unit vector along the radial direction. This allows us to rewrite Eq. (A4) as

$$\frac{\mathrm{Re}}{\Omega}\left|\frac{\ddot{b}(t)}{\dot{b}(t)}-\frac{\dot{b}(t)}{2b(t)}\right|\ll\left|\frac{12}{b(t)^2}\right|, \tag{A6}$$

leading to the validity condition of our study

$$\left|(1+b_1\sin\Omega t)\left[\frac{2\sin\Omega t+b_1(1+\sin^2\Omega t)}{24\cos\Omega t}\right]\right|\ll\frac{1}{\mathrm{Re}}. \tag{A7}$$

As long as this condition holds, we can safely neglect the inertial contributions in Eq. (A1) so that Darcy's law equation (4) perfectly describes the periodically driven flow we study. Notice that condition (A7) is not valid near the turning points, where the upper plate velocity vanishes ($\dot{b}\sim\cos\Omega t=0$). However, this is not a serious limitation since the system is stable around the points where $\dot{b}\to 0$ [see for instance Fig. 2].

Once a particular value of b_1 is considered, one should use Eq. (A7) to establish what range of values for Re can be used in order to validate Darcy's law formulation. The parameter Ω does not have a direct role since it appears in the argument of bounded periodic functions. In agreement with the studies performed in Refs. [1–10] we have verified that condition (A7) is perfectly valid in the low Reynolds number limit [$\lessapprox O(10^{-2})$], when the typical values of the dimensionless amplitude are used ($0.02\leq b_1\leq 0.2$) [11]. However, if inertial effects are important, as in the case of Ref. [11] we obtain a much larger Reynolds number [$15<\mathrm{Re}<60$], and obviously Eq. (A7) no longer holds.

Moreover, observe that the value of the dimensional frequency of oscillation ω cannot be arbitrarily large. This can be verified by inspecting Eq. (A7): if ω is increased, both Re and Ω assume larger values. As a result the right-hand side of Eq. (A7) will become increasingly smaller. On the other hand, the maximum value of the left-hand side will remain unchanged. In this case, condition (A7) would be eventually violated. Again, we stress that the key parameters to establish the validity of condition (A7) are Re and b_1.

Finally, as already pointed out in Sec. II our Darcy's law approach requires the system to be of large aspect ratio, meaning that $q\ll b(t)/R(t)$, where $b(t)/R(t)\ll 1$. In this work, as in Ref. [11] we use a value of q on the order of 10^2, which comfortably fulfills the large aspect ratio requirement.

[1] P. G. Saffman and G. Taylor, Proc. R. Soc. London, Ser. A **245**, 312 (1958).
[2] D. Bensimon, L. P. Kadanoff, S. Liang, B. I. Shraiman, and C. Tang, Rev. Mod. Phys. **58**, 977 (1986); G. M. Homsy, Annu. Rev. Fluid Mech. **19**, 271 (1987); K. V. McCloud and J. V. Maher, Phys. Rep. **260**, 139 (1995).
[3] L. Paterson, J. Fluid Mech. **113**, 513 (1981).
[4] M. J. Shelley, F.-R. Tian, and K. Wlodarski, Nonlinearity **10**, 1471 (1997).
[5] M. Ben Amar and D. Bonn, Physica D **209**, 1 (2005).
[6] C.-Y. Chen, C.-H. Chen, and J. A. Miranda, Phys. Rev. E **71**, 056304 (2005).
[7] A. Tatulchenkov and A. Cebers, Phys. Fluids **20**, 054101 (2008).
[8] D. Derks, A. Lindner, C. Creton, and D. Bonn, J. Appl. Phys. **93**, 1557 (2003).
[9] M. Tirumkudulu, W. B. Russel, and T. J. Huang, Phys. Fluids **15**, 1588 (2003).
[10] A. Lindner, D. Derks, and M. J. Shelley, Phys. Fluids **17**, 072107 (2005).
[11] S. N. Rauseo, Phys. Rev. E **62**, 8058 (2000).
[12] J. A. Miranda and M. Widom, Physica D **120**, 315 (1998).
[13] J. A. Miranda and E. Alvarez-Lacalle, Phys. Rev. E **72**, 026306 (2005).
[14] C.-Y. Chen, C.-H. Chen, and J. A. Miranda, Phys. Rev. E **73**, 046306 (2006).